UNIVERSITÄT AUGSBURG
Universitätsbibliothek

OPEN ACCESS
OPUS AUGSBURG

Towards fully automated inspection of large components with UAVs: offline path planning

Constantin Wanninger, Raphael Katschinksy, Alwin Hoffmann, Martin Schörner, Wolfgang Reif

Angaben zur Veröffentlichung / Publication details:

Wanninger, Constantin, Raphael Katschinksy, Alwin Hoffmann, Martin Schörner, and Wolfgang Reif. 2020. "Towards fully automated inspection of large components with UAVs: offline path planning." In *Proceedings of the 17th International Conference on Informatics in Control, Automation and Robotics - ICINCO, July 7-9, 2020*, edited by Oleg Gusikhin, Kurosh Madani, and Janan Zaytoon, 71–80. Setúbal: SciTePress. https://doi.org/10.5220/0009887900710080.

Nutzungsbedingungen / Terms of use:

CC BY-NC-ND 4.0

Dieses Dokument wird unter folgenden Bedingungen zur Verfügung gestellt: / This document is made available under these conditions:
CC-BY-NC-ND 4.0: Creative Commons: Namensnennung - Nicht kommerziell - Keine Bearbeitung
Weitere Informationen finden Sie unter: / For more information see:
https://creativecommons.org/licenses/by-nc-nd/4.0/deed.de

Towards Fully Automated Inspection of Large Components with UAVs: Offline Path Planning

Constantin Wanninger[a], Raphael Katschinsky, Alwin Hoffmann[b], Martin Schörner[c] and Wolfgang Reif

Institute for Software and Systems Engineering, University of Augsburg, Augsburg, Germany

Keywords: UAV, Visual Inspection, Trajectory Planning, Ant Colony Optimization.

Abstract: Automation mechanisms are increasingly established in the field of visual inspections. UAVs can be used for particularly large components, such as those used in ship production and for critical infrastructures. This paper concentrates on the problem of visual inspection in the field of perspective-dependent route planning. It is shown how the requirements for such a system can be implemented and elaborated. Furthermore we investigate how sensor positions can be calculated offline, based on optical and geometrical requirements and how a trajectory can be planned which contains the found sensor positions for each given area on the component. It is shown how the systems architecture can be designed in order to be able to adapt it to different requirements for the planning of sensor positions and trajectory. The implementation was tested in a simulation environment, evaluated using a benchmark data set and it was shown how above-average results can be achieved on this data set.

1 INTRODUCTION

The development progress and the strongly increased availability of unmanned aerial vehicles (UAVs) in the last years open up more and more possibilities for civil and scientific applications. For example, the use of UAVs for the inspection and measurement of infrastructures is being investigated, as they enable image-based observation from almost any perspective. Among others, the Competence Center Multicopter of (Deutsche Bahn AG, 2020) offers a comprehensive portfolio in the infrastructure sector. This includes the inspection of rail tracks, buildings and bridges as well as construction progress and condition documentation, to name just a few.

A still little explored area, is the fully automated visual inspection of large technical components by UAVs, to which this work is dedicated. The components considered here are assemblies according to DIN-199, i.e. self-contained objects consisting of at least two individual parts or assemblies of lower order. Currently, visual inspection of large technical components is still mostly carried out manually. For this purpose, an inspector checks the attached individual parts whether the present situation corresponds to the normal conditions of the component. This form of inspection, however, is associated with longer inspection times, increased personnel expenditure, human error susceptibility, and thus with overall increased financial costs, which can be addressed by the full automation of the visual inspection.

The offline path planning within a fully automated inspection is usually divided into two subproblems, finding sensor positions, so-called viewpoints, and finding a collision-free route through all viewpoints. When planning viewpoints, it must be ensured that they can be reached by the UAV and that no obstacles block the view of the component to be examined, or more generically expressed point of interest (POI). In order for a POI, e.g, to be optimally located in the picture, the desired resolution, focus and the camera's angle of aperture must be taken into account when choosing the location of the viewpoint in relation to the POI. When selecting the position, the orientation of the visual sensor to the normal of the POI must also be taken into account. However, this desired orientation cannot necessarily be achieved with a UAV, since the tilt and inclination angle of the UAV cannot be selected at will and the camera is statically attached to the copter or the degree of freedom of a

[a] https://orcid.org/0000-0001-8982-4740
[b] https://orcid.org/0000-0002-5123-3918
[c] https://orcid.org/0000-0001-6237-222X

Wanninger, C., Katschinsky, R., Hoffmann, A., Schörner, M. and Reif, W.
Towards Fully Automated Inspection of Large Components with UAVs: Offline Path Planning.
DOI: 10.5220/0009887900710080
In *Proceedings of the 17th International Conference on Informatics in Control, Automation and Robotics (ICINCO 2020)*, pages 71-80
ISBN: 978-989-758-442-8
Copyright © 2020 by SCITEPRESS – Science and Technology Publications, Lda. All rights reserved

swivel-mounted camera is limited. Therefore, it must be considered to what extent the angle between the normal of the POI and the vector of the optical axis of the camera may deviate. In addition, a minimum distance between the copter and the component may be required for safety reasons.

The route should contain all viewpoints from which all POIs can be inspected. Therefore, it is important to keep the route through all the viewpoints as short as possible and optimize the route lenght. Since the search for the shortest route in three-dimensional space is NP-hard (LaValle, 2006), procedures must be considered that offer an almost optimal solution for this problem in polynomial time. In the course of optimizing the route length, it is therefore important to keep the number of viewpoints as small as possible, while still ensuring an optimal view of all POIs.

This work is dedicated to exactly these two parts, the viewpoint and trajectory planning. This involves the fully automated inspection of predefined areas on the component. It is examined how viewpoints can be planned offline on the prerequisites mentioned above and a route based on them. The designed procedure is tested simulatively and the results of the trajectory planning are evaluated using benchmark data sets.

2 RELATED WORK

Work that is specifically dedicated to the fully automated inspection of technical infrastructures by UAVs usually aims to achieve complete visual coverage of the entire surface of the respective infrastructure, which is the aim of the *Coverage Path Planning* (Galceran and Carreras, 2013; Danner and Kavraki, 2000). A detailed summary of the current inspection scenarios provided by UAVs is provided by (Jordan et al., 2018). According to the work of (Bircher et al., 2015), the most adaptable approaches to the inspection scenario are those that use two-step optimization. In a first step, viewpoints are computed that cover the entire surface of the infrastructure, which can be achieved by solving the *Art Gallery problem* (O'Rourke, 1987; González-Banos, 2001). In a second step, a route or trajectory is calculated that connects all viewpoints, which can be modeled by solving the *Traveling Salesman Problem* (Laporte, 1992).

A concrete CPP solution for UAVs is described by (Bircher et al., 2015), in which the surface of the infrastructure is represented by a triangle mesh and a viewpoint is calculated for each triangle, from which the triangle is completely visible. In the second step a route through all viewpoints is planned. To do this, viewpoints are connected directly to each other if there is no obstacle between them, otherwise the RRT* search algorithm (Karaman and Frazzoli, 2011) is used to connect both viewpoints. RRT* is an extension of the *Rapidly Exploring Random Tree* (RRT) search algorithm by (LaValle, 2006).

(Englot and S. Hover, 2014) also show a two-step procedure for the inspection of ship hulls, which has already been successfully tested on the object. Although the procedure was designed for the use of autonomous underwater vehicles, it is still noteworthy because it deals with the automated offline planning of sensor positions relative to a component in three-dimensional space. In the first phase, configurations are randomly sampled by the *Redundant Roadmap Algorithm* until the surface is covered. In the second phase, an iterative solution of the RRT over all *goal-to-goal routes* calculates a route that connects all *goals*. Here, *goal-to-goal* means that the route ends at the configuration where it started. The *Local Coverage Algorithm (LCA)* optimizes the route in terms of length: Therefore (P,C) is the *set system*. The surface to be observed depends on a finite set of *geometric primitives* $p_i \in P$ (i.e., POIs to be covered) and from each configuration $q_j \in Q$ (i.e., a viewpoint) a set of p_i can be observed. The LCA is passed a *coverage route* W_G which is not yet optimized. The algorithm selects any goal $q_j \in W_G$ per iteration and tries to find a configuration $q_j^{'}$ that observes all *primitives*, that also observes q_j and at the same time reduces the costs for the route section $W_{q-1,q+1}$. Finding an optimized route stage is done by $RRT_{||}^{*}$, a variant of the RRT* algorithm by (Karaman and Frazzoli, 2011). To get an optimized route section $W_{q-1,q+1}^{'}$ with $q_j^{'}$ as intermediate configuration, $RRT_{||}^{*}$ will calculate in parallel an optimal collision free route from q_{j-1} to $q_j^{'}$ and one from $q_j^{'}$ to q_{j+1}. For this purpose two RRT* trees are built with q_{j-1} and q_{j+1} as the root. This method was evaluated at USCGC Seneca and it was shown that the feasible route with 192 viewpoints and 246 m could be improved to an optimized route with 169 viewpoints and 157 m length.

Works dealing with finding viewpoints usually assume that any pose of the camera can be taken. According to (Alarcon-Herrera et al., 2014) optimal viewpoints can be found for a POI if the optical axis of the camera runs along the normal vector of the POI and a so-called *standoff distance* to the POI is maintained. The *standoff distance* is calculated from the desired resolution of the POI in the image, the height and width of the image sensor and the angle of aperture of the camera. By aligning the optical angle along the normal of the POI, the POI is centered in the picture, which ensures maximum visibility of the POI.

This also prevents the POI from being distorted in the picture. By positioning the viewpoint around the *standoff distance* along the normal of the POI, an almost optimal resolution of the picture can be guaranteed. If a desired padding in pixels around the POI is desired, this can be taken into account in the calculation of the *standoff distance*.

(Malandrakis et al., 2018) present an already successfully tested procedure for the complete inspection of aircraft wings by penetration testing. For this purpose, a copter was equipped with a wide-angle camera with digital image stabilization and UV light. To ensure that the viewpoints are evenly distributed over the wing and that each area of the wing can be optimally inspected by the camera and UV light over the course of the trajectory, the viewpoints are planned so that the light cones from adjacent viewpoints overlap on the surface of the wing. The trajectory is then planned so that the copter travels row by row through all viewpoints.

3 CONCEPT

This chapter addresses the conceptual viewpoint and trajectory planning, in particular how the requirements for visual inspection of specified areas on the assembly can be achieved. As a basis, the required concepts are first introduced and then described how the position and orientation of a viewpoint can be planned depending on the camera's field of view. Finally, the concept behind trajectory planning is described, in which, for example, the *traveling salesman problem* can be solved with *Ant Colony Optimization*.

3.1 Orientation in Space

The calculation of the sensor positions and the trajectory planning is done in the coordinate space $\mathbb{R}^3$, which is based on a Cartesian coordinate system. The coordinate axes and coordinate frames follow the right-hand rule with the z-axis pointing upwards.

3.2 Workspace

The workspace is the *State-Space* (LaValle, 2006) considered here and builds on the underlying coordinate space. It defines the planning environment for the viewpoints and the trajectory. The size of the workspace is determined by the size of the component and any padding around it. The most important terms concerning the workspace are explained below.

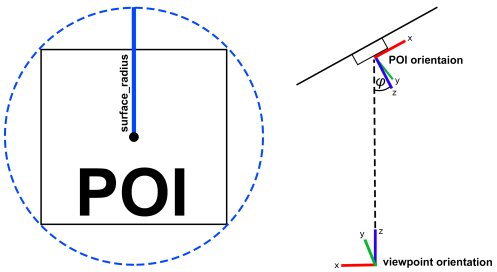

(a) (b)

Figure 1: (a) Example POI with corresponding surface radius. (b) Deviation angle φ between the normal of the POI and the optical axis of the camera.

3.3 Point of Interest

A Point-of-Interest, POI for short, is an individual part or a low-order assembly on the component to be inspected. POIs are described by its ID, position, orientation, maximum deviation angle, semantic Annotation and a surface radius. The position of the POI in the workspace is indicated by its coordinates x, y, z and its orientation x_q, y_q, z_q, w_q. The orientation of the copter is defined over the division ring of the quaternions $\mathbb{H}$. The position specifies the center of the POI. The maximum deviation angle φ_{max} specifies the maximum deviation of the angle φ between the normal of the POI and the optical axis of the camera, as shown in figure 1b. Each POI has a semantic annotation that describes the low-order part or component. To determine the camera position, the surface radius is also needed. It describes the radius of the POI on the surface of the part and is an approximation of the complex structure of the POI to a circle, as shown in figure 1a.

3.4 Viewarea

A POI is visible to the UAVs camera from a certain area, the so-called Viewarea. A Viewarea is calculated depending on the Angle-of-View (AoV) and the focus of the camera, as well as the surface radius of the POI to which the Viewarea is assigned. It is described by the radii va_{min} and va_{max}. Where va_{min} describes the minimum distance between the visual sensor and the POI. It indicates the lower limit from which a POI is no longer completely visible in the image. However, if the required minimum distance to the component is greater than this lower limit, va_{min} represents the required minimum distance to the component. The va_{max} represents the upper limit, from which on the POI is no longer visible in the picture. Both parameters thus indicate a lower and upper limit of the effectively usable viewarea.

3.5 Viewpoint

Each POI has at least one viewpoint from which sensor data can be collected. In the best case, it lies on the inverted z-axis of the camera orientation, fixed at the position of the POI. A viewpoint vp_i that observes a POI poi_j with associated viewarea VA_j is calculated so that $vp_i \in VP_i$. Here VP_i contains all viewpoints vp_i in the following form:

$$VP_i = \{vp_i \in VA_j : va_{min} \leq ||poi_j - vp_i||_2 \leq va_{max}\} \quad (1)$$

Furthermore, it can happen that two Viewareas are not disjoint, i.e. there is a set A with Viewareas $VA_i \supseteq VP_i$, $VA_j \supseteq VP_j$ and viewpoint $vp_i^{'}$, so that the following applies: $A = \{vp_i^{'} : vp_i^{'} \in VP_i \cap VP_j\}$. If A contains viewpoints that maintain the maximum angle of deviation φ_{max} for each POI they can theoretically observe, it is possible to use such sets A in the case of optimizing the trajectory length between three adjacent viewpoints. A viewpoint is described by its ID, position, orientation, a boolean parameter that indicates whether the viewpoint lies in the middle of its viewarea, three radii and a list of all POIs which it observes. The position is given by the coordinates x,y,z and the orientation by x_q,y_q,z_q,w_q. The orientation of the viewpoints is defined above the division ring of the quaternions $\mathbb{H}$. Position and orientation represent the position and orientation of the camera lens relative to the origin of the coordinate space. If the viewpoint cannot be optimally positioned (on the inverted z-axis of the camera orientation fixed to the position of the POI), the boolean parameter indicates that it is an alternative viewpoint. The radii vp_{min} and vp_{max} represent the effectively usable viewarea in the xy-plane at the viewpoint position, depending on the AoV of the camera. The radius r_φ represents the effective viewarea in the xy-plane at the viewpoint position, depending on the deviation angle φ of the POI.

3.6 Key Viewpoint

If at least one viewpoint is found for each POI, the number of viewpoints should be kept to a minimum. As described in the previous paragraph, alternative viewpoints can be calculated that can inspect more than one POI. However, this may result in a worse view on the POIs that $vp_i^{'}$ observes. Therefore, a good trade-off between optimal viewpoint positions and trajectory length must be found in the course of optimization. In the end there should be at most one viewpoint for each POI that observes it. The set of these viewpoints are the so-called key viewpoints.

3.7 Trajectory

A UAV has so-called holonomic properties, i.e. its controllable degree of freedom with respect to its position corresponds to its total degree of freedom with respect to its position. Therefore viewpoints can be accessed directly and the trajectory between two viewpoints can be described as a linear motion (LIN). For this purpose, this paper assumes that there are no obstacles between two adjacent viewpoints. Finally, the trajectory contains a permutation of all key viewpoints and represents a shortest route.

3.8 Planning of Viewpoints

Before the trajectory can be calculated, viewpoints must be planned depending on the camera's field of view. The following section describes the requirements that need to be considered when planning viewpoints and how viewpoints can be planned in detail:

3.8.1 Requirements for Viewpoint Planning

As stated by Alarcon et al. (Alarcon-Herrera et al., 2014), a POI is optimally positioned in the image if the optical axis of the camera runs along the normal vector of the POI and a *standoff-distance* to the POI is maintained (here: $va_{min} \leq standoff\ distance \leq va_{max}$). Since the tilt and inclination angle of the UAV is not arbitrary selectable and the camera is statically attached to the UAV, viewpoints have to be found so that φ (see figure 1b) is within the given tolerance range φ_{max} and the *standoff-distance* is kept.

3.8.2 Planning

When planning a viewpoint, the radii of the viewarea to a POI must be calculated and the orientation of the camera must be taken into account. The minimum- and maximum distance va_{min}, va_{max} between the viewarea and a POI is calculated as follows:

$$va_{min} = \frac{poi_i^r}{tan(\frac{min(AoV)}{2})} \quad (2)$$

$$va_{max} = f \cdot \frac{(poi_i^r \cdot \phi)^2[mm]}{A_{poi}[px]} \quad (3)$$

Where f is the focal length of the camera, A_{poi} the minimum size of the POI in pixels in the picture so that the POI can be identified and poi_i^r the surface radius of Poi poi_i. The constant ϕ indicates to which extent A_{poi} may be exhausted.

To examine the planning of the viewpoints under ideal conditions first, the orientation of the POIs and the camera was chosen so that the optical axis of the

camera runs along the normal vector of the POI and is therefore valid:

$$\forall vp_i, poi_i(vp_i, poi_i) \in VP_i \times POI_i \Rightarrow \varphi = 0 \quad (4)$$

Where POI_i is the set of all POIs for a single part or an assembly of lower order. VP_i is the set as described in Eq.1. If the z-axes of the camera, POI and workspace are parallel to each other, the orientation of the camera can be taken as the orientation of the viewpoint. The position of the viewpoint is then a translation around the *standoff-distance* along the z-axis of the POI. Thus the POI is located on the optical axis of the camera and the viewpoint is located in the middle of the viewwarea. The radii of the Viewarea at the position of the viewpoint are calculated as follows:

$$\begin{aligned} &vp_{max}(poi_i, vp_j) = \\ &= tan(\frac{max(AoV)}{2}) \cdot d(poi_i, vp_j) - poi_i^r \end{aligned} \quad (5)$$

$$\begin{aligned} &vp_{min}(poi_i, vp_j) = \\ &= tan(\frac{min(AoV)}{2}) \cdot d(poi_i, vp_j) - poi_i^r \end{aligned} \quad (6)$$

$$\begin{aligned} r_\varphi(poi_i, vp_j) = \\ = tan(\varphi_{max}) \cdot d(poi_i, vp_j) - poi_i^r \end{aligned} \quad (7)$$

$$d(poi_i, vp_j) = ||poi_i - vp_j||_2 \quad (8)$$

The radii vp_{min} and vp_{max} are especially important if a POI cannot be identified from a viewpoint during the inspection. If a POI cannot be identified from a POI during inspection, one of the radii can be used during inspection to circle around the viewpoint in a spiral flight. If the POI still cannot be identified, it will be marked as not present.

3.9 Planning the Trajectory

After key viewpoints have been found for all POIs, a trajectory containing all key viewpoints must be planned. For this purpose, the following describes which requirements have to be considered when planning a trajectory and how these can be fulfilled by modelling the *Travelings-Salesman-Problem* as *Ant Colony Optimization*.

3.9.1 Requirements for Trajectory Planning

For the offline planning of the trajectory there are three main requirements: For each POI to be inspected, each key viewpoint must be located on the trajectory. For easy handling of the UAV during the inspection, the trajectory should end at the position where it started. To minimize the time needed for the inspection, the trajectory through all key-viewpoints should be planned as short as possible.

3.9.2 Planning

The *Ant Colony Optimization* (ACO), a method for solving the *Travelings-Salesman-Problem*, was used to fulfill the requirements. This method is particularly well suited for a large number of nodes (viewpoints) because it provides a near-optimal solution (Chaudhari and Thakkar, 2019), as shown in table 1. Furthermore, a near-optimal route can be found in a short time by using ACO.

ACO is inspired by the behaviour of ants in finding a shortest possible route from their nest to a food source. For this purpose, ants leave pheromones on their route when they have found a food source. Other ants follow this pheromone trail with a certain probability, whereby the probability increases with the intensity of the pheromone on the trail. After a certain time, more and more ants follow the strongest/optimal pheromone trail. Since more pheromones can be deposited in the same time on a shorter route than on a longer one, the intensity of the pheromone trace increases most on the shorter route. Over time, the intensity of the pheromone trace of less used routes decreases again.

Table 1: Source: Chaudhari et al. (Chaudhari and Thakkar, 2019). Comparison of average and best found distances (in km) of *Ant Colony Optimization* (ACO), *Particle-Swarm-Optimization* (PSO), *Artificial-Bee-Colony* (ABC), *Firefly Algorithm* (FA) and *Genetic Algorithm* (GA). Burma14 represents 14 cities in Burma, Bayg29 29 cities in Bavaria and Att48 cities in the USA.

Algorithm	Route	Few of the benchmark TSPs		
		Burma14	Bayg29	Att48
ACO	Average	31,05	9274,79	35043,34
	Best	30,88	9195,22	34600,71
PSO	Average	32,34	15047,83	109979,87
	Best	30,88	14036,75	91237,09
ABC	Average	32,36	17404,62	107883,76
	Best	30,88	16658,30	101985,88
FA	Average	31,80	14283,51	81182,32
	Best	30,88	13062,40	78479,69
GA	Average	31,49	11023,70	50753,50
	Best	30,88	10018,10	46362,05

To imitate this behavior, first define the pheromone update formula (Eq. 9) for each edge c_{ij} in a graph $G = (V, E)$.

$$\tau_{ij} = (1 - \rho) \cdot \tau_{ij} + \sum_{k=1}^{m} \Delta\tau_{ij}^k \quad (9)$$

Where ρ is the pheromone evaporation rate, m the number of ants and $\Delta\tau_{ij}^{k}$ (Eq. 10) the pheromone intensity left by ant k at edge c_{ij}.

$$\Delta\tau_{ij}^{k} = \begin{cases} \frac{Q}{L_k} & if\ c_{ij}\ is\ on\ the\ Route\ of\ ant\ k \\ 0 & else \end{cases} \tag{10}$$

Where Q is a constant and L_k is the route length of ant k in the current iteration. The probability of taking the edge c_{ij} at node i to node j is given by Eq. 11.

$$p_{ij}^{k} = \begin{cases} \frac{\tau_{ij}^{\alpha} \cdot \eta_{ij}^{\beta}}{\sum_{c_{il} \in N(s^p)} \tau_{il}^{\alpha} \cdot \eta_{il}^{\beta}} & if\ c_{ij} \in N(j^p) \\ 0 & otherwise \end{cases} \tag{11}$$

Where j^p is the route taken by ant k so far and $N(j^p)$ are the edges (i,l) to not yet visited nodes l. The parameters α, β control the influence of the pheromone τ_{ij} and the heuristic information η_{ij} (Eq.12).

$$\eta_{ij} = \frac{1}{d_{ij}} \tag{12}$$

In this work the *Ant Colony System* (ACS) (Gambardella and Dorigo, 1996; Stuetzle and Dorigo, 1999; Dorigo et al., 1999), a variation of the ACO, was used. With ACS, only pheromone from the globally best ant is deposited on an edge c_{ij} and the pheromone update formula changes to a Global Pheromone Update Formula (Eq.13).

$$\tau_{ij} = (1-\rho) \cdot \tau_{ij} + \rho \cdot \Delta\tau_{ij}^{best} \tag{13}$$

Additionally, a local pheromone update formula (Eq. 14) is defined for each ant. This makes already visited edges less interesting for other ants and increases the exploration of not yet visited edges.

$$\tau_{ij} = (1-\rho) \cdot \tau_{ij} + \rho \cdot \tau_0 \tag{14}$$

$$\tau_0 = \frac{1}{n \cdot L_{nn}} \tag{15}$$

Where n is the number of key viewpoints and L_{nn} is the length of a route according to the *nearest neighbor heuristic*. In addition, formula (Eq. 11) is reformulated to calculate the probability of which node will be visited next by ant k. For this purpose, $q \in [0,1]$ is randomly determined and q_0 is fixed as a constant. The constant q_0 determines whether the focus should be on the exploration of G or the exploitation of good pheromone traces. Ant k then selects the next node j, according to the formula (Eq. 16)

$$j = \begin{cases} \underset{c_{ij} \in N(j^p)}{\operatorname{argmax}} \{\tau_{ij} \cdot \eta_{ij}^{\beta}\} & if\ q \le q_0 \\ J & otherwise \end{cases} \tag{16}$$

$$p_{ij}^{k} = \begin{cases} \frac{\tau_{ij} \cdot \eta_{ij}^{\beta}}{\sum_{c_{il} \in N(s^p)} \tau_{il} \cdot \eta_{il}^{\beta}} & if\ c_{ij} \in N(j^p) \\ 0 & otherwise \end{cases} \tag{17}$$

Here J is a random node j which has not yet been visited by ant k and according to Eq. 17: This calculation gives preference to nodes that are connected to the current node i by a short edge and have a high pheromone intensity.

The underlying graph $G = (V,E)$ is a complete graph, i.e. each key viewpoint is connected to each by an edge. Since the trajectory consists of LINs between the key-viewpoints, the edge weights are equal to the Euclidean distance between the key-viewpoints.

4 REALIZATION AND IMPLEMENTATION

This chapter deals with the realization and implementation of the concept presented in chapter 3. For the realization of the offline planning of the viewpoints and the trajectory a software architecture was developed, which allows to define different requirements to the viewpoint and trajectory planning and to extend the system component by component. For trajectory planning, it is shown how the *Ant Colony System* can be implemented.

4.1 System Architecture

The elaboration of all presented concepts was abstracted to a necessary level in order to first investigate the suitability of UAVs for fully automated inspection of given areas on the component. The design of the system was therefore chosen in such a way that the realization within the scope of this paper is limited to the complete concept and can be extended beyond that. For this reason, the software architecture placed great emphasis on the scalability and interchangeability of the viewpoint and trajectory planning components with the aim of adapting the system to different viewpoint and trajectory requirements. If, for example, a trajectory is to be planned for multiple components of the same type, a strategy can be selected that keeps the length of the trajectory as short as possible, thus saving time and costs in visual inspection. If, on the other hand, a trajectory is to be planned for individual components, a much less computationally intensive strategy can be used to plan the trajectory if a fast calculation of the trajectory is essential. In order to plan viewpoints and trajectory, camera parameters, minimum distance of the UAV to the component

and the desired planning strategy are transferred to the system. The camera parameters necessary for the system are the orientation of the camera lens relative to the orientation of the UAV, angle of view, focal length and the desired minimum size of a POI in the image in pixels. The strategy for viewpoint and trajectory planning is then instantiated via an abstract factory. Which factory should be used is determined by the implementation of the strategy pattern: The strategy for viewpoint planning is determined using the transferred parameters and the corresponding factory is selected. If a new strategy is to be added to the system, a new factory can be added by implementing the corresponding interface. The system outputs the trajectory and the key viewpoints in serialized form. Afterwards the planned trajectory can be tested simulatively with ROS, Gazebo and Rviz or the key viewpoints can be sent to a UAV via mavlink.

4.2 Viewpoint and Trajectory Planning

The viewpoint and trajectory planning component were realized and implemented in Python 3. The exact elaboration is described below.

4.2.1 Viewpoint Planning

When planning the viewpoints, the radii were calculated according to the formulas in chapter 3.8.2. To calculate the position of the viewpoint, the x and y position of the POI was taken and the position of the viewpoint along the z-axis of the POI was shifted by the *va_max_radius* of the associated viewarea. The *va_max_radius* distance between the viewpoint and the POI was chosen to allow the UAV to initially maintain a certain safety distance to the component. The orientation of the camera has been adopted as the viewpoint orientation. This is possible for the case under consideration because the z-axis of the workspace, the optical axis of the camera and the normal of the POI are parallel to each other.

4.2.2 Trajectory Planning

The implementation of the ACS is based on the concept of Trevlovett (trevlovett,). The implementation of the ACS is multithreaded, i.e. each ant was implemented as a single thread. The distance between the key viewpoints and the pheromone intensity on the edges are created as two separate matrices. The Euclidean distance between the key-viewpoints is used as the distance measure, since the trajectory is defined as LINs between the key-viewpoints. The pheromone intensity on each edge is initially set to τ_0:

$$\tau_0 = \frac{1}{\frac{1}{2N} \cdot \sum_{c_{ij}} ||i-j||_2} \tag{18}$$

where N is the number of key viewpoints. The calculation of the global and local pheromone update formula was done as in Eq. 13 and Eq. 14 and the heuristic information η_{ij} as in Eq. 12. The formula for the pheromone intensity at edge c_{ij} was calculated as follows:

$$\Delta\tau_{ij}^{best} = \frac{||i-j||_2^{best}}{L_k^{best}} \tag{19}$$

Where $||i-j|||_2^{best}$ is the Euclidean distance of the edge c_{ij} on the best route and L_k^{best} is the distance of the best route.
The implementation of the formula as in Eq. 17, was implemented as a roulette wheel-style selection procedure. This is done by taking the average value of the pheromone and heuristic information of all edges $c_{il} \in N(j^p)$:

$$avg = \frac{\sum_{c_{il} \in N(s^p)} \tau_{il} \cdot \eta_{il}^{\beta}}{N^R} \tag{20}$$

Where N^R is the number of viewpoints not yet visited. The edge to the first viewpoint in the list of unvisited viewpoints whose pheromone and heuristic information value of the edge is greater than *avg* is taken. The implementation is based on the ROS infrastructure and can be visualized with Rviz. Gazebo was used to simulate the behavior of the UAVs and the visual sensors. For illustrative purposes we provide videos of the implementation of the simulation environment as well as the processing of the trajectory (ros, ; rvi,).

5 EVALUATION

For the evaluation, nine POIs were considered, which are attached to a component. The orientation of the POIs were chosen so that their normals are parallel to the z-axis of the workspace. For the additional evaluation of the trajectory planning, the results of the implementation were evaluated using a TSP-benchmark data set. The trajectory through the nine key viewpoints was tested with Gazebo, Rviz and ROS. The results of the evaluation are shown below.

5.1 Results of Trajectory Planning

As described in chapter 3.9, the trajectory is planned in a complete graph $G = (V,E)$. For each of the nine POIs, a viewpoint has been planned which is located in the middle of the POI's Viewarea. The optical axis of the camera is always on the normal of the POI, so

that for all pairs $(vp_i, poi_i) \in VP_i \times POI_i$ the deviation angle φ is 0. An almost optimal route of 11.78 meters through all nine key viewpoints was found after twenty iterations of the procedure described in section 4.2.2. The found route in G, as well as the course of the route through all key viewpoints including the associated POIs, their normals and the z-orientation of the key viewpoints can be seen in figure 2.

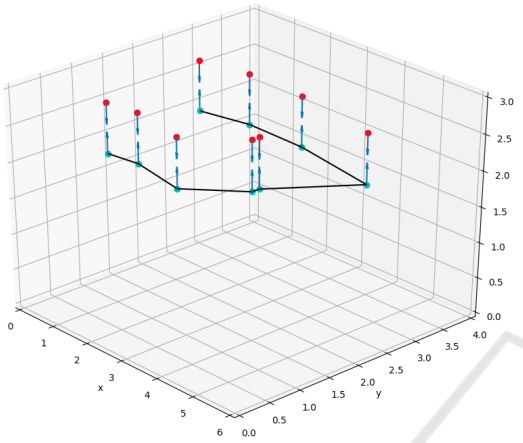

Figure 2: Planned trajectory through all key viewpoints to their corresponding POIs. The vectors of the POIs correspond to the z-orientation and those of the viewpoints to the optical axis of the camera.

5.1.1 Evaluation of the ACS Implementation

The implementation of the ACS was evaluated on the Att48 benchmark dataset. (att,) Att48 consists of the distance relationships between 48 cities in the USA. For the number of ants, as well for the parameters β and ρ the results of the work of Pettersson et al. (Pettersson and Lundell Johansson, 2018) are used:

$$\beta = 5, \quad \rho = 0{,}5, \quad m = \lfloor 0{,}3 \cdot N \rfloor \tag{21}$$

Where m is the number of ants and N is the number of key viewpoints. The implementation was evaluated using the Att48 dataset and it was examined which ratio of ants to iterations yields a good trade-off of found distance to required computing time. The number of iterations was calculated based on the number of ants, which in turn, as in Eq. 21, depends on the number of key viewpoints. For this purpose, the value $\lfloor \frac{2000}{m} \rfloor$ by Pettersson et al. (Pettersson and Lundell Johansson, 2018) were used and examined to what extent better results can be achieved by increasing the number of iterations. The values $\lfloor \frac{2000}{\frac{m}{i}} \rfloor$ for $i \in \{2,3,4,5,6,7\}$ were tested. With each value, ten passes were performed. The average result for each value can be seen in Table 2. The best distance on the Att48 record of 34023.35 km was achieved with

Table 2: Comparison of the results with different choice of iterations.

Att48		
iterations	∅ lenght [in km]	∅ time [in s.]
2000 / (m / 2)	36483.416	84.262
2000 / (m / 3)	35937.116	124.487
2000 / (m / 4)	36261.336	173.377
2000 / (m / 5)	36031.142	217.897
2000 / (m / 6)	36061.551	247.518
2000 / (m / 7)	35929.504	293.229

$\lfloor \frac{2000}{\frac{m}{7}} \rfloor$ iterations. This result undercuts the result obtained by Chaudhari et al. The course of the best distance found in this work on the Att48 data set is shown in figure Although the best results were obtained with $\lfloor \frac{2000}{\frac{m}{7}} \rfloor$ iterations, no significant better results were obtained by increasing the iterations beyond $\lfloor \frac{2000}{\frac{m}{2}} \rfloor$.

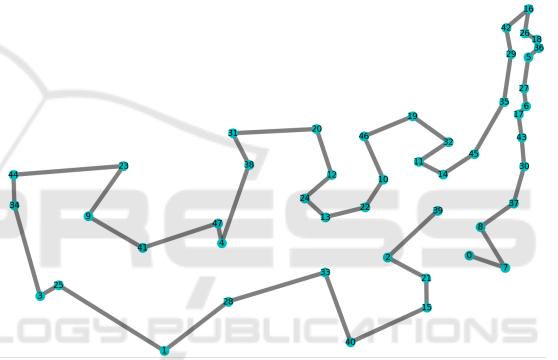

Figure 3: Course of the route for the distance of 34023.35 km.

5.2 Results in Simulation

To check the trajectory in the simulation, the trajectory, consisting of the nine key viewpoints, was transferred to the ROS node. As can be seen in figure 4, the trajectory could be followed through the nine key viewpoints. Here it can be observed that the movement between the key viewpoints is not always linear. The exact reason for this is unknown, but it is most likely due to the local-planner, which requires several attempts to get to the viewpoint using *Adaptive Monte Carlo Localization*. Another reason could be the defined speed of the UAV. It was observed that the higher the speed was defined, the longer it took the UAV to reach a viewpoint. Since the deceleration behavior of the UAV was not defined near a viewpoint, it is possible that the UAV flies over viewpoints, then decelerates and tries to reach the viewpoint again. This procedure may be repeated several times.

SCITEPRESS
SCIENCE AND TECHNOLOGY PUBLICATIONS

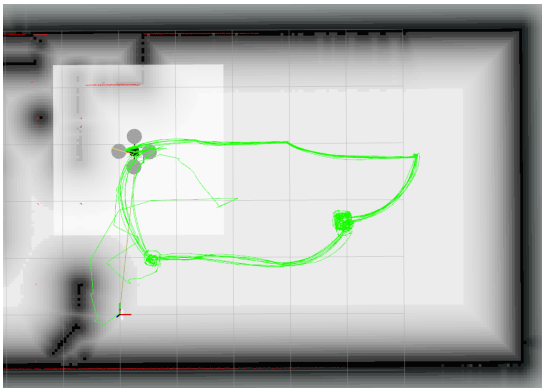

Figure 4: Performed trajectory in the simulation.

6 CONCLUSION AND FUTURE WORK

Within the scope of this paper the feasibility of offline trajectory planning for fully automated visual inspection of predefined areas on a component was investigated. It was shown how viewpoints to predefined parts on the component can be planned and what has to be considered during the planning. The planning of viewpoints was examined for the use of UAVs. Furthermore, it was shown how the *Ant-Colony-System* can be used to plan a trajectory that contains all key-viewpoints and can be planned in short time and has a nearly optimal length. However, a number of milestones still need to be reached before fully automated visual inspection can be performed by UAVs for large components:

First of all, the planning of optimal viewpoints of any orientation of the POIs has to be more investigated.If the maximum deviation radius allows the viewpoint to be off the optical axis, it is important to check how to plan viewpoints that observe multiple POIs simultaneously and shorten the overall trajectory length. Furthermore, it must be possible for the system to evaluate viewpoints that have already been found offline: First of all, it must be checked whether a viewpoint is located in the area of a static obstacle on the component, whether the field of view on the POI is blocked by a static obstacle or whether the viewpoint is otherwise not accessible by the UAV. Also, light conditions and shading can make it difficult to inspect a POI. It is therefore necessary to investigate how to take into account difficult inspection conditions when planning offline and how to plan viewpoints so that difficult conditions can be dealt with more easily during the inspection.

In section 3.8, a strategy was presented for how to proceed if a POI cannot be identified from a viewpoint during the inspection. However, this is only one way to deal with such a situation. It is also possible to consider procedures that already plan and provide alternative viewpoints to a POI offline. Furthermore, when inspecting predefined areas of the component, the *Coverage Planning* must also be considered. This is necessary if geometrically complex and/or large POIs on the part are to be inspected and a single viewpoint per POI is no longer sufficient.

The existence check examined in this paper is only one use case for the inspection of predefined areas on the component. Further use cases, which have to be investigated in the future, are the relative orientation of a POI in the component, as well as the attachment of the POI to the component.

There are also areas of trajectory planning that can be optimized. As in viewpoint planning, obstacles must also be taken into account when planning the trajectory. Therefore it must be possible to check in the context of trajectory planning whether adjoining key viewpoints can be reached by a linear trajectory of the UAV and how the obstacles between adjoining key viewpoints can be avoided. Another point of optimization is the current view of the trajectory as LINs between the key viewpoints. Depending on the inspection scenario, point-to-point or trajectory control could also be considered.

The automated visual inspection of large components by UAVs is still in its infancy, but it is a necessary step to make visual inspections of components more precise, easier and more efficient in the future.

REFERENCES

Localization using laser-based slam. last access: 29.03.20.

Mp-testdata - the tsplib symmetric traveling salesman problem instances. last access: 25.04.20.

Trajectory trough all viewpoints. last access: 29.03.20.

Alarcon-Herrera, J. L., Chen, X., and Zhang, X. (2014). Viewpoint selection for vision systems in industrial inspection. In *2014 IEEE International Conference on Robotics and Automation (ICRA)*, pages 4934–4939.

Bircher, A., Alexis, K., Burri, M., Oettershagen, P., Omari, S., Mantel, T., and Siegwart, R. (2015). Structural inspection path planning via iterative viewpoint resampling with application to aerial robotics. In *2015 IEEE International Conference on Robotics and Automation (ICRA)*, pages 6423–6430.

Chaudhari, K. and Thakkar, A. (2019). Travelling salesman problem: An empirical comparison between aco, pso, abc, fa and ga. In Shetty, N. R., Patnaik, L. M., Nagaraj, H. C., Hamsavath, P. N., and Nalini, N., editors, *Emerging Research in Computing, Information, Communication and Applications*, pages 397–405, Singapore. Springer Singapore.

Danner, T. and Kavraki, L. E. (2000). Randomized planning for short inspection paths. In *Proceedings 2000 ICRA. Millennium Conference. IEEE International Conference on Robotics and Automation. Symposia Proceedings (Cat. No.00CH37065)*, volume 2, pages 971–976 vol.2.

Deutsche Bahn AG (2020). Kompetenzcenter Multicopter DB.

Dorigo, M., Caro, G. A. D., and Gambardella, L. M. (1999). Ant algorithms for discrete optimization. *Artificial Life*, 5:137–172.

Englot, B. and S. Hover, F. (2014). Sampling-based coverage path planning for inspection of complex structures. *ICAPS 2012 - Proceedings of the 22nd International Conference on Automated Planning and Scheduling*.

Galceran, E. and Carreras, M. (2013). A survey on coverage path planning for robotics. *Robotics and Autonomous Systems*, 61:1258–1276.

Gambardella, L. M. and Dorigo, M. (1996). Solving symmetric and asymmetric tsps by ant colonies. In *Proceedings of IEEE International Conference on Evolutionary Computation*, pages 622–627.

González-Banos, H. (2001). A randomized art-gallery algorithm for sensor placement. *Proc. 17th ACM Symp. Comp. Geom.*, pages 232–240.

Jordan, S., Moore, J., Hovet, S., Box, J., Perry, J., Kirsche, K., Lewis, D., and Tse, Z. T. H. (2018). State-of-the-art technologies for uav inspections. *IET Radar, Sonar Navigation*, 12(2):151–164.

Karaman, S. and Frazzoli, E. (2011). Sampling-based algorithms for optimal motion planning. *The International Journal of Robotics Research*, 30(7):846–894.

Laporte, G. (1992). The traveling salesman problem: An overview of exact and approximate algorithms. *European Journal of Operational Research*, 59:231–247.

LaValle, S. M. (2006). *Planning Algorithms*. Cambridge University Press.

Malandrakis, K., Savvaris, A., Domingo, J. A. G., Avdelidis, N., Tsilivis, P., Plumacker, F., Fragonara, L. Z., and Tsourdos, A. (2018). Inspection of aircraft wing panels using unmanned aerial vehicles. In *2018 5th IEEE International Workshop on Metrology for AeroSpace (MetroAeroSpace)*, pages 56–61.

O'Rourke, J. (1987). *Art Gallery Theorems and Algorithms*. Oxford University Press, Inc., New York, NY, USA.

Pettersson, L. and Lundell Johansson, C. (2018). Ant colony optimization - optimal number of ants.

Stuetzle, T. and Dorigo, M. (1999). Aco algorithms for the traveling salesman problem.

trevlovett. Python ant colony tsp solver. last access: 10.10.2019.

SCITEPRESS SCIENCE AND TECHNOLOGY PUBLICATIONS